MEASUREMENT OF GAS BUBBLES IN MERCURY USING PROTON RADIOGRAPHY

B. W. Riemer [a], P. R. Bingham [a], F. G. Mariam [b], F. E. Merrill [b]

[a] *Spallation Neutron Source / ORNL, P. O. Box 2008, Bldg. 8600, MS 6473, Oak Ridge, TN 37831,* riemerbw@ornl.gov
[b] Los Alamos National Laboratory

An experiment using proton radiography on a small mercury loop for testing gas bubble injection was conducted at the Los Alamos Neutron Science Center (LANSCE) in December 2006. Small gas bubble injection is one of the approaches under development to reduce cavitation damage in the U.S. Spallation Neutron Source mercury target vessel. Several hundred radiograph images were obtained as the test loop was operated over range of conditions that included two jet type bubble generators, two needle type bubble generators, various mercury flow speeds and gas injection rates, and use of helium, argon and xenon. This paper will describe the analysis of the radiograph images and present the obtained bubble measurement data.

I. INTRODUCTION

Short beam pulse liquid metal spallation targets may be vulnerable to cavitation damage of their target vessels which could adversely limit target lifetime and operating power.[1] The U. S. and Japanese Spallation Source projects (SNS, JSNS) both employ liquid mercury circulating in stainless steel vessels and their targets and are design to operate at MW power levels. Operational experience at high power has yet to be achieved in the projects' early stages, but research and development on the cavitation damage issue is already under way. The goal is to develop technologies that mitigate cavitation damage such that it limits neither target lifetime (more that radiation damage) nor operating power. Higher proton beam power will provide greater neutron intensity to facility users.

One damage mitigation strategy under development is to inject small gas bubbles into the mercury. The idea is that the population of small bubbles could absorb and / or attenuate the pressure wave generated by the short and intense proton beam pulse used for the spallation reaction. The characteristics of the bubble population required to be effective are a subject of R&D, but diameters of about 10 to 100 μm in sufficient number density to establish a void fraction of 0.1 to 0.5% is the current goal. Creating a bubble population like this is challenging, and progress has been impeded by the lack of credible diagnostics to quantify small gas bubble populations in liquid mercury.

While development of useful laboratory diagnostics is a concurrent goal of the SNS R&D program, an experiment using proton radiography at the Los Alamos Neutron Science Center (LANSCE) was conducted in 2006 that successfully imaged injected gas bubbles in a mercury test loop.[2] Hundreds of static radiographs and several radiograph movies were obtained while operating the loop and bubble generators over a range of gas injection rates and mercury flows. Quantifying the bubble populations was essential to understanding bubble generator performance.

Two approaches have been used on the radiographs to obtain the bubble volume and equivalent diameter: a bubble edge detection method; an integrated transmission method. The methods will be described and results presented for a limited number of test conditions. Comparison between methods will also be made, as well as with data obtained from acoustic emissions from bubble generation.

II. EXPERIMENT DESCRIPTION

A brief description of the experiment is included as it is more thoroughly described elsewhere.[2] A small mercury test loop originally used in cavitation damage experiments called the In Beam Bubble Test Loop (IBBTL) was prepared for the radiography tests with the addition of a second jet bubbler and small needle bubblers (as needed).[3] A photograph of the loop (sans most instrumentation) is shown in Fig. 1. The radiography object location was at the removable components called Damage Test Specimens (DTS); these could be configured to provide the nominal mercury thickness or to reduce it to 6 mm for improved image contrast. The DTS also allowed for the installation of needle bubblers directly in the field of view; the needles could be oriented either coaxially with mercury flow or perpendicular to it.

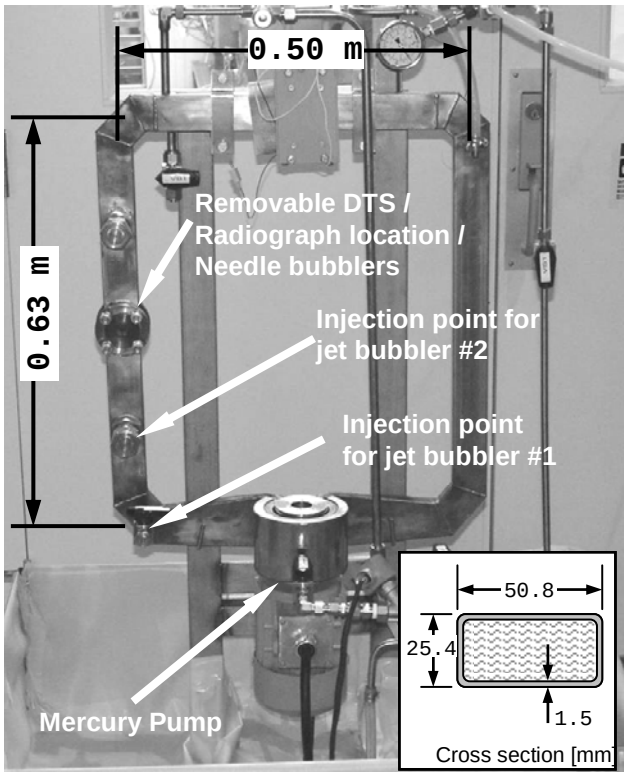

Fig. 1. Photo of the IBBTL showing its approximate dimensions. This is prior to installation of instrumentation and secondary equipment. Mercury circulated in the clockwise direction for the experiment.

Fig. 2 shows the needle bubbler for used for coaxial orientation with mercury flow. The needle was made from type 316 stainless steel and with an outside diameter of 200 µm and inside diameter of 100 µm. The mounting flange was made of aluminum and coated with protective paint. The flange part that protruded into the mercury flow had an outside diameter of 29 mm with the inside bored to a diameter of 25 mm. Wall thickness along the proton path was 1.65 mm.

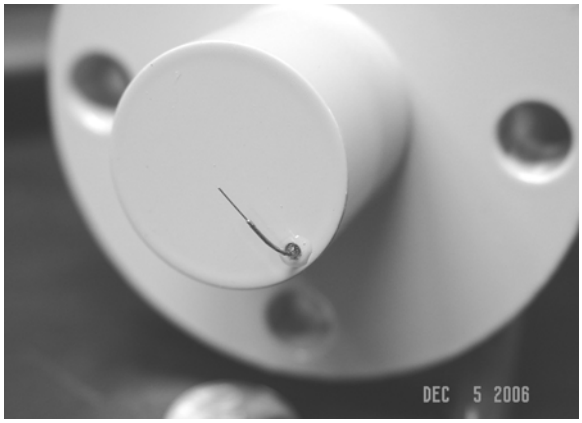

Fig. 2. Needle bubbler for orientation coaxial with mercury flow.

Fundamental descriptions of the proton radiography technique can be found in Refs. 4-6. It was known that density contrast would be the limiting factor for identifying bubbles in this experiment; this was the motivation for enabling 6 mm mercury thickness as well as using aluminum for the DTS. LANSCE proton radiography (pRad) employs an array of imaging cameras that can be simultaneously or sequentially triggered. During this experiment static images were of primary interest, so most often multiple cameras were triggered simultaneously. This allowed for image averaging and improved signal to noise ratios. Initial testing indicated the minimum resolvable bubble diameter to be about 300 µm.

Jet bubblers injected gas into the loop at locations upstream of the DTS / radiography object location. These were expected to produce a spectrum of bubble sizes but prior attempts to quantify sizes in mercury had failed. Typically helium was the injected gas but argon and xenon were also tried. Loop operation with the jet bubblers varied mercury flow from 0.27 to 0.67 L/s with gas injection rate from 50 to 500 standard cubic centimeters per minute (sccm).

Needle bubblers were expected to produce more regular size bubbles. Theoretical predictions for bubble sizes produced from coaxially oriented needle had been applied previously to an X-ray experiment by Kogawa with stagnant mercury.[7] It was hoped to confirm Kogawa's measurement and expand into the flow regime. Tested mercury velocities at the needle tip included 0.38, 0.63 and 0.96 m/s; gas injected rate ranged from 0.1 to 250 sccm.

III. RADIOGRAPH ANALYSIS METHODS

Images provided by the LANSCE proton radiograph group have already been pre-processed. Multiple camera images from the array were aligned, averaged and normalized to a no-bubble plus dark field condition image. Images were in tagged image file format (TIFF).

The two methods for calculating bubble volume are described in the following subsections. For both methods a series of processing steps were performed to first locate bubbles within the image. Due to the number of images taken during this experiment, a semi automated method for bubble detection was developed using MatLab.[8] This method first runs a detection algorithm to locate candidate bubbles and then allows the user to remove any bubbles that can be identified as noise (streaking in images, bubbles in normalization, bubbles on edge of field of view, etc.). The interface also allows the user to select areas containing bubbles that were missed during the initial phase. An automated segmentation is performed on such regions to find the bubbles of interest. Missed

bubbles were typically caused by intensity fluctuations across the image or by merging with adjacent bubbles.

Automated bubble detection involved 3 major steps: low pass filtering, thresholding, and morphological filtering. The low pass filter is Gaussian, and was used to remove pixel noise in the images.

Over the image sets obtained during this experiment, a single threshold could not be used to segment the bubbles. Instead a threshold level was calculated for each image. First, an attempt is made to remove any large bubbles from the threshold calculation by masking out any pixels greater than 3 standard deviations above the mean for pixel value in the region of interest. Then the threshold at 3 standard deviations above the mean for the remaining pixels is calculated. This thresholding step results in a binary image of the bubbles.

Bubbles were segmented in this binary image by grouping bubble pixels that were neighbors. A set of morphological features were calculated for each bubble in the image. These features were centroid, area, eccentricity, major axis, minor axis, and bounding box.

Two morphological filters were used on these results. The first removed any bubbles containing 20 or fewer pixels. The second removed bubbles having a ratio of major axis to minor axis greater than 10. This filter removed segmented regions resulting from streaking due to shift out noise in the cameras and artifacts from the image array alignment pattern.

Obtaining the volume of the bubbles was a key goal of the experiment. From the two dimensional proton radiographs, the bubble volumes were estimated through two methods. The first method used the detected edges of the bubbles, and the second integrated over the transmission values inside a bubble area.

III.A. Edge Detection Method

In the edge detection method, the binary image of each segmented bubble was used to make the volume calculation. This image is represented by the checked blob in the top of Fig. 3. Bubble volume was estimated using each horizontal row of image pixels within the bubble boundary and assuming the rows are circular disks with diameter equal to the row width "B", so that each row volume was $(1)\pi(B/2)^2$ cubic pixels. The row volumes were summed for each bubble and converted to cubic mm. To accurately convert to mm, a measurement of pixels across the diameter of the DTS was made for each series of measurements. The inside diameter of the DTS was known to be 25.4mm. This resulted in pixel sizes of approximately 55 μm.

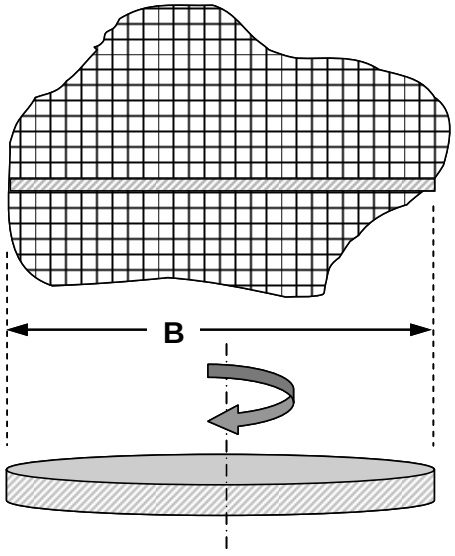

Fig. 3. The edge detection approach for bubble volume assumed each horizontal row of pixel is a circular disk of diameter B and one pixel high. Disk volumes were summed for each bubble and scaled to mm^3.

III.B. Integrated Transmission Method

The intensity of pixels in a proton radiograph is determined by the attenuation and scattering of the protons passing through the materials at the object location. While three dimensional calculations can be difficult to make for more complex objects, this test essentially consisted of an aluminum channel containing mercury. The only dynamics involved were the replacement of mercury by helium when a bubble was present as illustrated in Fig. 4. Normalization was performed on the images by setting regions without bubbles (with intensity I_0) equal to zero by first dividing all pixels by I_0 and subtracting the resulting value from 1. This resulted in a change in transmission for each pixel. The graph and equation shown in Fig. 5 were then used to convert this change in transmission intensity to a bubble thickness in mm.

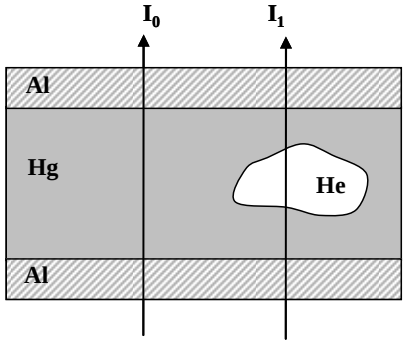

Fig. 4. Transmission cross section in the experiment. Difference between I_1 and I_0 is used to calculate bubble thickness along each ray.

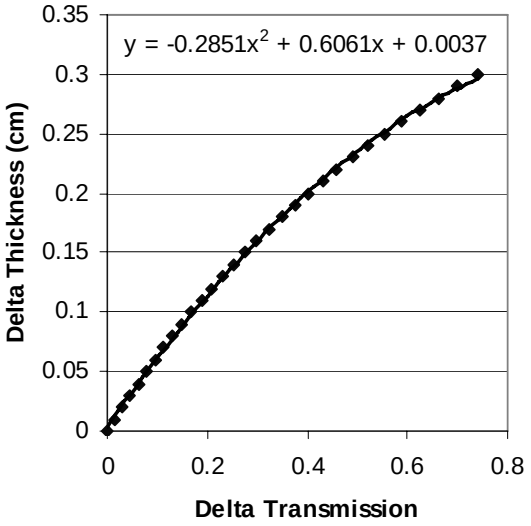

Fig. 5. Conversion of transmission change to bubble thickness.

The simple model used to estimate transmission versus thickness in a proton radiograph is given in equation 1. Here, λ is the nuclear interaction length, θ_c is the radiographic cut angle (0.01 radians for these experiments), θ_o is the multiple coulomb scattering angle introduced by the object of thickness *l*. Gaussian multiple Coulomb scattering with an angular distribution of width θ_o was assumed as given by equation 2. In equation 2, *p* is the proton momentum, β is the relativistic velocity and x_o is the radiation length of the material. The aluminum was accounted for along with the mercury in the radiation and nuclear interaction lengths.

This model of transmission versus thickness was used to calculate the data points in Fig. 5. For convenience these were fit to a polynomial in the region of interest. The polynomial fit was used to determine bubble thickness in the radiograph analysis.

$$T = e^{-\frac{l}{\lambda}}\left(1 - e^{-\left(\theta_c^2 / 2\theta_o^2\right)}\right) \qquad (1)$$

$$\theta_o = 14.1 / p\beta\sqrt{l/x_o} \qquad (2)$$

IV. RESULTS

Example jet bubbler images are shown in Fig. 6 for two conditions along with graphics showing identified bubble areas from the edge analysis. Both images were obtained looking through 22 mm of mercury flowing at 0.47 L/s and helium gas injected at 140 sccm. Fig. 6A is from bubbler #2 operating, while 6B was is from bubbler #1. The jet bubblers were identical in internal construction, but bubble #1 discharged its bubbly mixture through a 3.5 mm diameter tube 108 mm long before entering the main loop flow some 290 mm upstream of the DTS. Bubbler #2's discharge tube was only 25 mm long and its mixture entered the main loop 150 mm upstream of the DTS. It can be seen that the available image contrast is quite different. Although the image in 5B was considerably poorer it was possible to detect most of what appear to be bubbles in the image. A few, however, could have been missed (circled features).

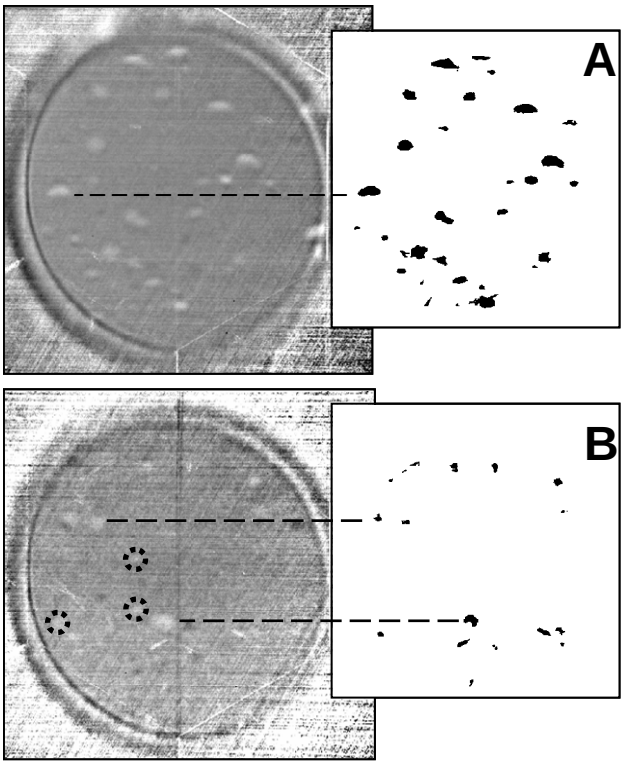

Fig. 6. Example jet bubbler radiographs, both through 22 of mercury flowing at 0.47 L/s and helium gas injected at 140 sccm. (A) was with bubbler #2; (B) was with bubbler #1. Bubble areas identified by the edge detection are shown to the right. While bubbles were well identified in (A), poor contrast in (B) may have led to some bubbles being missed.

Data obtained by the edge method was used to produce the bubble size histogram is shown in Fig. 7. In this example, the populations between helium, argon and xenon are compared with bubbler #2 and fixed mercury flow and gas injection rates. This data was compiled from ten radiographs of each condition. Helium produced somewhat more of the smaller bubble sizes. The smallest bubble identified had an equivalent diameter of 240 μm.

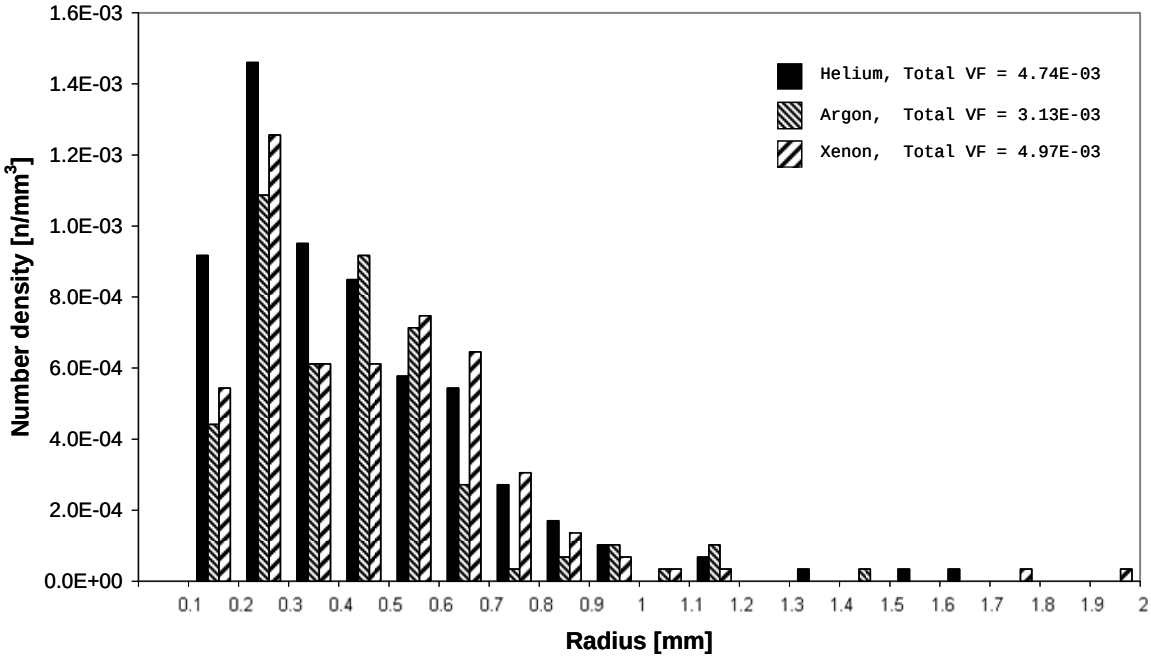

Fig. 7. Example bubble size histogram from data obtained using the edge method for three jet bubbler conditions. Each used bubbler #2 and with 6 mm mercury thickness flowing at 0.44 L/s. The three gas species were injected at 140 sccm. Total gas void fraction (VF) is also shown.

While all images have been analyzed with the edge detection method, the transmission method for bubble volume has only been applied to needle bubbler images. Example analyzed coaxial needle bubble radiographs are shown in Fig. 8. Here the processed images show the mask area for analysis behind the detected bubbles. The result of this step appears the same regardless of volume analysis method. Bubble equivalent diameter – based on volume for a spherical bubble – show noticeable differences. Fig. 9 plots the estimated average bubble diameters from this bubbler over a range of helium injection rates for three mercury velocities (U_L). While agreement is roughly good between edge and transmission results, differences close to 50% are seen for some conditions. Unfortunately this translates to difference in bubble volume of about three.

Also included in Fig. 9 is diameter based on acoustic emissions from bubble generation. Sound recordings were made prior to proton radiography using a microphone placed on the outside of the DTS. Emissions associated with bubbles separating from the needle could be clearly distinguished for most of the test space. Gas flow was established by calibrated mass flow controllers so that bubble volume could be determined with the observed generation period. Equivalent bubble diameter was adjusted for the gas flow difference caused by the controller's standard temperature and pressure conditions and those in the loop during the experiment, as well as for the effect of surface tension on bubble pressure. These adjustments typically made for about a 6% bubble diameter reduction.

V. DISCUSSION

Image analysis was able to locate and determine bubble edges with minimal manual intervention. The fidelity of bubble volume and equivalent diameter estimation is somewhat uncertain. In general, the edge method gives larger bubble sizes compared to the transmission method. There are limited regions of good agreement in particular with stagnant mercury conditions. The edge method result for 10 sccm and stagnant mercury is oddly off its general trend, but it is close to the 2.9 mm value obtained by Kogawa than the other methods.

The assumption of section circular symmetry used in the edge volume estimate cannot be validated over the full range of conditions examined here. The transmission approach should be more robust as it eliminates this simplifying assumption. Certainly it gives results closer to those based on sound emissions. There seems to be fewer sources of potential error with the acoustic method.

While bubble edges appear to be well identified, actual bubble edge positions cannot be precisely seen in these radiographs. As one approaches the real bubble edge the influence of gas on transmission along the proton path becomes diminishingly smaller and below resolvable levels. This further suggests advantage to the transmission method over the edge method.

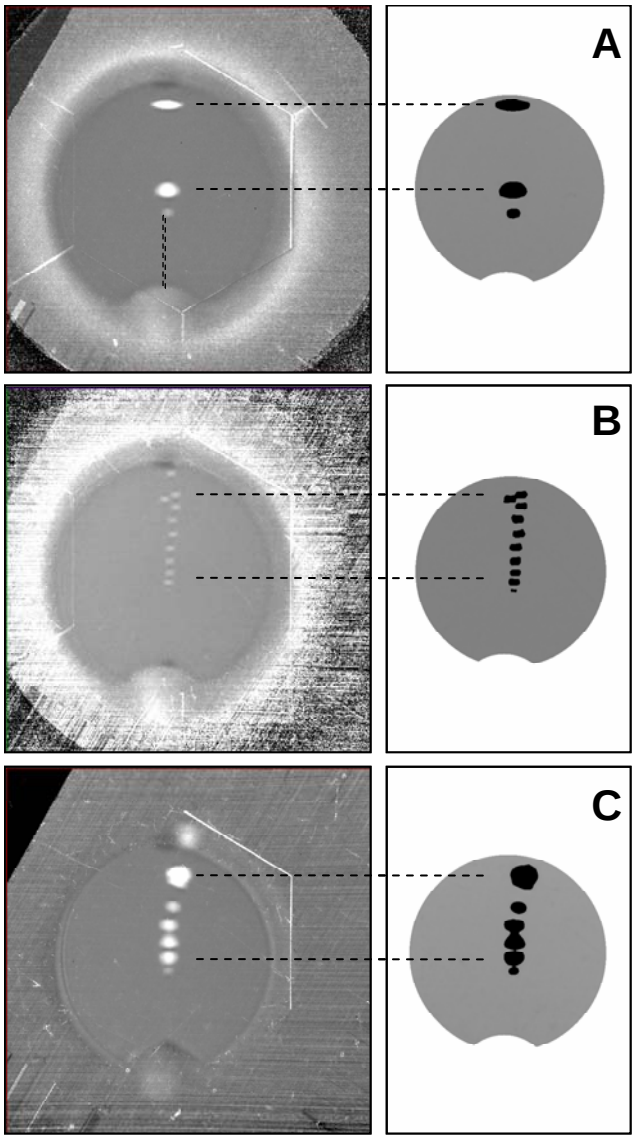

Fig. 8. Coaxial needle bubbler example radiographs with detected bubbles to the right. (A) Stagnant mercury with 10 sccm helium; (B) 10 sccm helium with 0.63 m/s mercury velocity; (C) 100 sccm helium with 0.63 m/s mercury velocity. (A) Includes a sketched-in needle for reference.

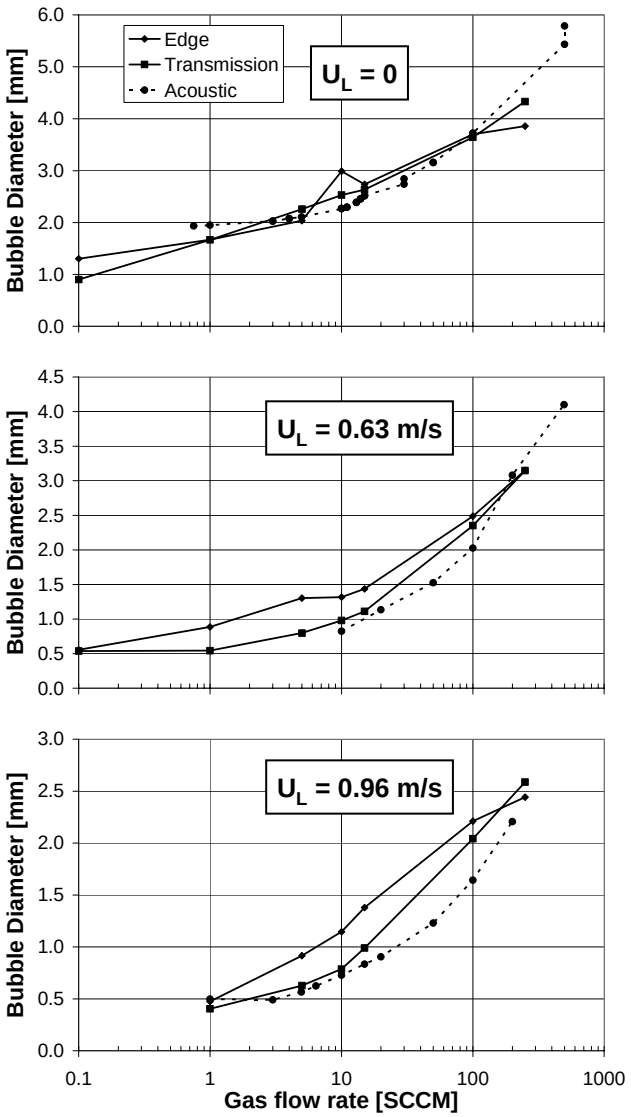

Fig. 9. Bubble diameter as determined by the edge and transmission methods from radiographs for coaxial needle generated bubbles. Also included are data determined from acoustic emissions from bubble generation and known helium gas flow rates. Three mercury velocities (U_L) are shown.

The smaller bubble sizes associated with flowing mercury have made accurate volume measurement from the radiographs more difficult.

VI. CONCLUSIONS

The use of proton radiography has for the first time provided credible data that quantifies the size, number density and void fraction of injected gas bubbles in mercury. Useful radiograph images were obtained through significant thicknesses of mercury and over a broad range of mercury flow rates and gas injection rates. The size distribution data has allowed evaluation of jet bubbler performance heretofore not possible. Bubble production from needles has been quantified; the results are contributing to development and benchmarking of two-phase computational fluids dynamics simulations needed for cavitation damage mitigation R&D program goals.[9, 10]

ACKNOWLEDGMENTS

ORNL/SNS is managed by UT-Battelle, LLC, for the U.S. Department of Energy under contract DE-AC05-00OR22725.

This work has benefited from the use of the Los Alamos Neutron Science Center at the Los Alamos National Laboratory. This facility is funded by the US Department of Energy.

REFERENCES

1. J. R. HAINES, B.W. RIEMER, D. K. FELDE, J.D. HUNN, S.J. PAWEL, *Journal of Nuclear Materials*, **343**, 58-69 (2005).
2. B. W. RIEMER, D. K. FELDE, M. W. WENDEL, F. G. MARIAM, F. E. MERRILL, "Proton Radiography Experiment to Visualize Gas Bubbles in Mercury", *18th Meeting of the International Collaboration on Advanced Neutron Sources*, Dongguan, Guangdong, P R China, April 25-29, 2007, http://www.icans-xviii.ac.cn/ (2007).
3. B. RIEMER, J. HAINES, M. WENDEL, G. BAUER, M. FUTAKAWA, S. HASEGAWA, and H. KOGAWA, "Cavitation Damage Experiments for Mercury Spallation Targets at the LANSCE – WNR in 2005", *Proc. Spallation Materials Technology 8*, Taos, NM, October 2006. Submitted to the Journal of Nuclear Materials for publication.
4. N.S.P. KING et al., Nuclear Instruments and Methods in Physics Research A, **424** 84-91 (1999).
5. C. T. MOTTERSHEAD and J. D. ZUMBRO, "Magnetic Optics for Proton Radiography", *Proc. 1997 Particle Accelerator Conf.*, Vancouver 1397 (1997).
6. G. E. HOGAN et al. "Proton Radiography", *Proc. 1999 Particle Accelerator Conf.*, New York 579 (1999).
7. H. KOGAWA, T. SHOBU, M. FUTAKAWA, A. BUCHEERI, K. HAGA, T. NAOE, "Effect of wettability on bubble formation at gas nozzle under stagnant condition", *Proc. Spallation Materials Technology 8*, submitted to the Journal of Nuclear Materials for publication.
8. http://www.mathworks.com/products/matlab/
9. A.A. IBRAHIM, D. FELDE, B. RIEMER and M. WENDEL, "CFD Validation of Gas Injection into Stagnant Water", *Proc. 5th Joint ASME / JSME Fluids Engineering Conference*, San Diego, CA, USA. 2007
10. M. WENDEL, A.A. IBRAHIM, D. FELDE, and B. RIEMER, "Gas Injection into Stagnant and Flowing Mercury" 2007, *5th Joint ASME / JSME Fluids Engineering Conference*, San Diego, CA, USA. 2007